

Kolmogorov-Hinze scales in turbulent superfluids

Tsuyoshi Kadokura¹ and Hiroki Saito¹

¹*Department of Engineering Science, University of Electro-Communications, Tokyo 182-8585, Japan*
(Dated: January 7, 2021)

When a two-component mixture of immiscible fluids is stirred, the fluids are split into smaller domains with more vigorous stirring. We numerically investigate the sizes of such domains in a stirred two-component superfluid in a fully-developed turbulent state with energy-input rate ϵ . For the strongly immiscible condition, the typical domain size is shown to be proportional to $\epsilon^{-2/5}$, as predicted by the Kolmogorov-Hinze theory in classical fluids. For the weakly immiscible condition, quantum effects become pronounced and the power changes from $-2/5$ to $-1/4$. The domain size scaled by the interface thickness collapses into a universal line.

When oil is poured into water and these fluids are stirred, the oil becomes split into droplets in the water. The droplet sizes become smaller with more vigorous stirring. Such disintegration phenomena in multicomponent fluids are ubiquitous in nature, and are important in engineering and industry.

Kolmogorov [1] and Hinze [2] considered the disintegration process of droplets, and estimated the size of droplets in turbulent fluids. In fully-developed turbulence, the energy is input into the system as large-scale eddies that cascade toward a smaller scale, resulting in the Kolmogorov power law of the energy spectrum [3]. In such turbulent fluids, large-size droplets are unstable because they are fragile to deformation and disintegration due to the fluctuating pressure of the surrounding fluid. Small droplets are thus produced by the breakup of large droplets, and this breakup process continues to a scale where the turbulent energy to break up the droplets becomes balanced with the droplet energy sustaining its shape. Droplets smaller than this scale coalesce into large droplets. Therefore, there exists a characteristic size D of droplets in turbulent fluids, which is referred to as the Kolmogorov-Hinze (KH) scale, given by [2]

$$D \sim (\sigma/\rho)^{3/5} \epsilon^{-2/5}, \quad (1)$$

where σ is the interface tension coefficient, ρ is the density of the surrounding fluid, and ϵ is the energy input rate to maintain the turbulence. The KH scale has been experimentally verified in various systems [4–8]. Furthermore, direct numerical simulations have been performed over the last decade [9–14].

In this Letter, we extend the study of KH scales to a quantum mechanical system: the superfluid turbulence of a two-component Bose-Einstein condensate (BEC). We will show that the KH scale also appears in this superfluid system and is modified by quantum effects. Turbulent behavior in superfluids has been widely studied. For single-component superfluids, an isotropic fully-developed turbulent state exhibits the Kolmogorov power law [15–20]. The turbulent behavior of gaseous BECs has also been experimentally studied [21–23], and a power law behavior has been observed recently [24–27]. A wide variety of systems have been studied theoretically, such as two-dimensional systems [28–32], dipolar superfluids [33], and

boundary layers [34]. Here, we focus on the turbulence in a two-component BEC. Turbulence in multicomponent BECs has been investigated by many researchers [35–41]. In the context of domain-size scaling in multicomponent BECs, coarsening dynamics following domain formation have been studied extensively [42–52]. However, the KH scale, i.e., domain-size scaling in conjunction with the Kolmogorov turbulence, has not yet been investigated.

The KH scale in Eq. (1) is derived as follows. In a turbulent fluid, a domain undergoes fluctuating pressures that vary over its size D , which causes deformation and disintegration of the domain. This pressure difference over the size D can be expressed as $\sim \rho v^2 \equiv P_{\text{turbulence}}$, where v is the velocity difference of the surrounding fluid over the size D . Within the inertial range of an isotropic homogeneous turbulence, the statistical average of v^2 obeys the Kolmogorov two-thirds law [3], $v^2 \propto (\epsilon D)^{2/3}$, and hence $P_{\text{turbulence}} \sim \rho(\epsilon D)^{2/3}$. On the other hand, a domain tends to sustain its shape and resist disintegration. This sustaining force arises from the interface tension, and the pressure required to deform the domain is thus estimated to be $\sim \sigma/D \equiv P_{\text{sustain}}$ [53]. Breakup of domains to smaller sizes stops at the scale that satisfies

$$P_{\text{sustain}} \sim P_{\text{turbulence}}, \quad (2)$$

which gives the KH scale in Eq. (1).

For an immiscible two-component BEC, the interface tension, which arises from the interatomic interaction and quantum pressure, is well-defined, as in classical fluids [54–56]. Therefore, we expect that the KH scale in Eq. (1) also emerges in two-component BECs when the thickness of the interface W is much smaller than the domain size D . However, when W is comparable to or larger than D , the picture of the interface tension breaks down in the derivation of Eq. (1). The interface thickness W is determined by the competition between the quantum pressure and the intercomponent repulsion, and W becomes large when the former dominates the latter. Thus, in the limit of large W , the mechanism to sustain domains against disintegration originates mainly from the quantum pressure $P_{\text{sustain}} \sim \hbar^2/(mD^2)$ instead of $P_{\text{sustain}} \sim \sigma/D$, where m is the mass of an atom. In this case, Eq. (2) gives the characteristic size as

$$D \sim (\hbar/m)^{3/4} \epsilon^{-1/4}. \quad (3)$$

Therefore, in the limit of weak segregation with large W , the quantum mechanical effect becomes pronounced and the KH scale is expected to change from the $-2/5$ to $-1/4$ power law with respect to ϵ . In the remainder of this Letter, we will corroborate this prediction using numerical simulations of the coupled Gross-Pitaevskii (GP) equations.

In the mean-field approximation, a two-component BEC is described by the coupled GP equations,

$$(i - \gamma)\hbar \frac{\partial \psi_1}{\partial t} = \left(-\frac{\hbar^2}{2m} \nabla^2 + V_{\text{ext}} + g_{11}|\psi_1|^2 + g_{12}|\psi_2|^2 - \mu_1 \right) \psi_1, \quad (4a)$$

$$(i - \gamma)\hbar \frac{\partial \psi_2}{\partial t} = \left(-\frac{\hbar^2}{2m} \nabla^2 + V_{\text{ext}} + g_{22}|\psi_2|^2 + g_{12}|\psi_1|^2 - \mu_2 \right) \psi_2, \quad (4b)$$

where $\psi_j(\mathbf{r}, t)$ is the macroscopic wave function of the j th component, $V_{\text{ext}}(\mathbf{r}, t)$ is the external stirring potential, and $g_{jj'} = 4\pi\hbar^2 a_{jj'}/m$ with $a_{jj'}$ being the s -wave scattering length between the j th and j' th components. The constant γ in Eq. (4) introduces dissipation of energy from the condensate into thermal atoms [57]. The value of γ is selected in such a way that the energy dissipation occurs predominantly below the scale of the healing length and does not affect the dynamics in the inertial range. The chemical potential μ_j is adjusted to maintain the unitarity, i.e., $\int |\psi_j|^2 d\mathbf{r}$ is conserved.

The miscibility between the two components is determined by the coupling coefficients $g_{jj'}$. The two superfluids are immiscible and phase separation occurs when $g_{12}^2 > g_{11}g_{22}$ is satisfied [58]. In the following, we assume $g_{11} = g_{22} \equiv g > 0$ and $g_{12} > 0$; therefore, the immiscible condition reduces to

$$g_{12} > g. \quad (5)$$

The phase separation of immiscible components produces an interface, at which excess energy arises, resulting in the interface tension. For $g_{12}/g - 1 \ll 1$, the interface tension coefficient is given by [54–56]

$$\sigma \simeq \left[\frac{\hbar^2 n^3}{2m} (g_{12} - g) \right]^{1/2}, \quad (6)$$

where n is the number density far from the interface. The thickness W of the interface between two components, over which each density changes from 0 to n (or n to 0), has the form

$$W \simeq \xi (g_{12}/g - 1)^{-1/2}, \quad (7)$$

where $\xi = \hbar/(2mgn)^{1/2}$ is the healing length.

The length, time, and wave functions are normalized by ξ , $\hbar/(gn)$, and \sqrt{n} , respectively, where n is taken to be an average density of each component. In this

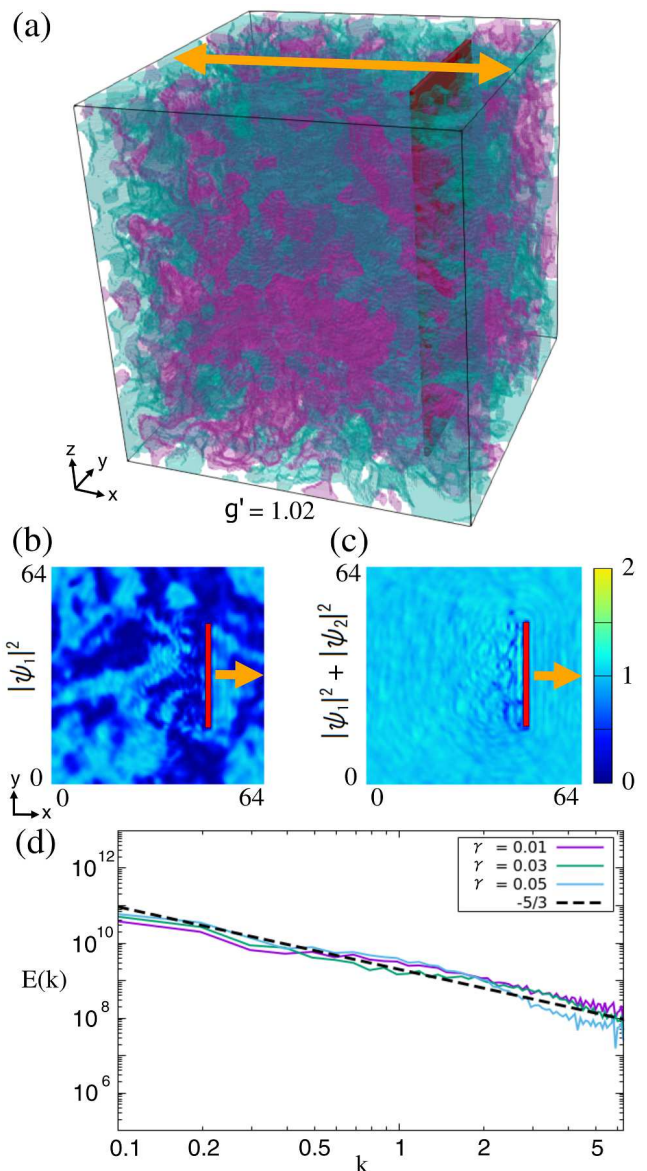


FIG. 1. A two-component BEC is stirred by a plate-shaped potential (red or black) to generate a turbulent state. (a) Snapshot of a fully-developed turbulent state at $t = 2000$ for $g' \equiv g_{12}/g = 1.02$ and $\nu_{\text{plate}} = 0.0048$. Isodensity surfaces of $|\psi_1|^2 = 0.5$ (purple or dark gray) and $|\psi_2|^2 = 0.5$ (green or light gray) are shown. The arrow indicates the range of sinusoidal motion of the stirring potential. (b)-(c) Cross-sectional views of $|\psi_1|^2$ and $|\psi_1|^2 + |\psi_2|^2$ at $z = 32$. The arrows indicate the direction of the potential motion. (d) Energy spectra $E(k)$ (arbitrary unit) for $\gamma = 0.01, 0.03$, and 0.05 , averaged over $t = 1900-2000$. The dashed line has a slope of $-5/3$. See the Supplemental Material for a movie of the dynamics [60].

unit, the interaction coefficients appear in the normalized GP equation only through $g_{12}/g \equiv g'$. We consider a box of size $L^3 = 64^3$ with a periodic boundary condition, in which the two components are equally populated, $\int |\psi_1|^2 d\mathbf{r} = \int |\psi_2|^2 d\mathbf{r} = L^3$. To generate the turbulent state, the system is stirred by a plate-shaped potential

V_{ext} with a size of $1 \times 32 \times 64$ and a potential height of 10. This plate-shaped potential is moved sinusoidally over the system ($0 < x < L$) at a frequency ν_{plate} , as shown in Fig. 1(a), which can input the turbulent energy into the large scale. The coupled GP equations (4) are numerically solved using the pseudospectral method [59]. The space is discretized into a 128^3 mesh and the time step is typically 10^{-3} . The initial state has uniform density with random phases on each mesh.

The two-component BEC is stirred until the fully-developed turbulent state is achieved. Figure 1(a) shows isodensity surfaces of $|\psi_1|^2$ and $|\psi_2|^2$ at $t = 2000$ for $g' = 1.02$ and $\nu_{\text{plate}} = 0.0048$. The immiscible condition (5) is satisfied for this value of g' ; therefore, the two components are separated and domains are formed in each component. Figure 1(a) shows that the domain sizes are typically $\gtrsim 10$, while $W \simeq (1.02 - 1)^{-1/2} \simeq 7$ from Eq. (7). The KH scale is thus expected to be marginally in the region of Eq. (1) (rather than Eq. (3)) with this condition, which will be investigated later. Figures 1(b) and 1(c) show cross-sectional views of the densities $|\psi_1|^2$ and $|\psi_1|^2 + |\psi_2|^2$, respectively, where the stirring potential is moving rightward at this moment. Although the density $|\psi_1|^2$ (or $|\psi_2|^2$) largely varies in space due to the phase separation (Fig. 1(b)), the total density far from the stirring potential is almost uniform (Fig. 1(c)). The small density holes in Fig. 1(c) indicate that quantized vortices are generated behind the potential moving at almost the sound velocity of the density wave. To confirm that the system has reached the Kolmogorov turbulence, we calculate the energy spectrum $E(k)$ of incompressible velocity field [15] averaged over the duration of $t = 1900$ -2000 for $\gamma = 0.01, 0.03$, and 0.05 , which is shown in Fig. 1(d). The slope of the logarithmic plot of $E(k)$ agrees well with the Kolmogorov power law of $-5/3$ within the inertial range of the wave number ($k \lesssim 2$). In this range, the lines in Fig. 1(d) are almost independent of the dissipation constant γ , which indicates that, for these values of γ , the energy dissipation occurs predominantly at the small length scale and does not affect the dynamics in the inertial range. In the following calculations, we take $\gamma = 0.03$.

The following procedure is used to numerically evaluate the typical size of the domains. We first discretize the density-imbalance distribution as

$$d(\mathbf{r}) = \begin{cases} 1 & (|\psi_1(\mathbf{r})|^2 \geq |\psi_2(\mathbf{r})|^2) \\ -1 & (|\psi_1(\mathbf{r})|^2 < |\psi_2(\mathbf{r})|^2), \end{cases} \quad (8)$$

which eliminates the information of the interface thickness and small excitations, and enables the information of only the domain size to be extracted. Figures 2(a)-2(c) show snapshots of the distributions of $d(\mathbf{r})$. Fourier transformation of $d(\mathbf{r})$ is performed and its azimuthal average in the \mathbf{k} space is taken, which we denote as $\tilde{d}(k)$. Figure 2(d) shows the time evolution of $\tilde{d}(k)$ for the dynamics in Fig. 1. Since the initial state has a random phase on each mesh, $\tilde{d}(k)$ is initially independent of k . The distribution of $\tilde{d}(k)$ then tilts toward small

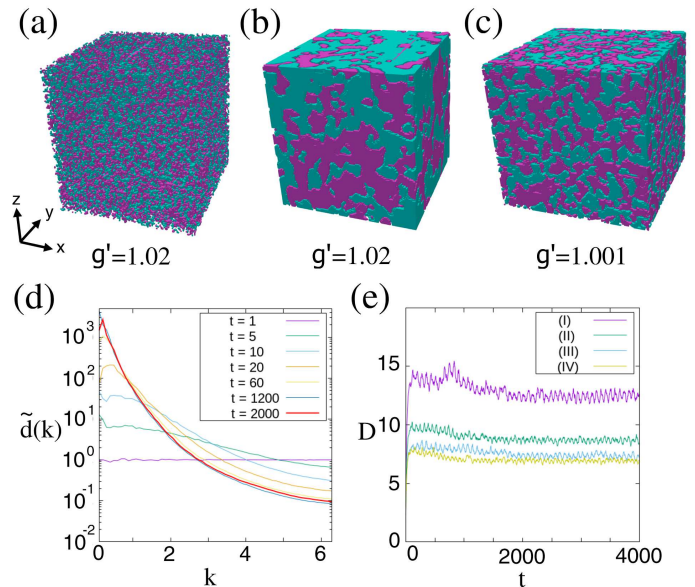


FIG. 2. Discretized density distributions $d(\mathbf{r})$ in Eq. (8) at (a) $t = 1$ for $g' \equiv g_{12}/g = 1.02$, (b) $t = 2000$ for $g' = 1.02$, and (c) $t = 2000$ for $g' = 1.001$. (d) Time development of the radial wave-number distribution $\tilde{d}(k)$ for $g' = 1.02$. In (a)-(d), $\nu_{\text{plate}} = 0.0048$. (e) Time development of the typical domain size $D \equiv 2\pi/[\int k\tilde{d}(k)dk/\int \tilde{d}(k)dk]$ for $(g', \nu_{\text{plate}}) = (1.02, 0.0032)$, $(1.02, 0.0048)$, $(1.01, 0.0048)$, and $(1.001, 0.0048)$, which are labeled as (I), (II), (III), and (IV), respectively.

wave numbers, and the steady distribution is reached for $t \gtrsim 1200$. We have confirmed that the steady distribution of $\tilde{d}(k)$ does not depend on the initial state. The first moment of $\tilde{d}(k)$, $\int k\tilde{d}(k)dk/\int \tilde{d}(k)dk \equiv \langle k \rangle$, gives a typical wave number in the density distribution, and thus $2\pi/\langle k \rangle \equiv D$ characterizes the size of the domains. Figure 2(e) shows the time development of D for different values of g' and ν_{plate} . The size D in the steady state decreases with g' and with an increase in ν_{plate} . This is because the interface tension (6) decreases with g' and the energy input rate increases with ν_{plate} .

To study the KH scale quantitatively, we need to calculate the rate ϵ at which the energy is input into the system by the stirring potential. Let the position of the plate-shaped potential be $x_{\text{plate}}(t)$, which moves in the $\pm x$ direction, as shown in Fig. 1. The force acting on the potential from the superfluid is then $F = -\partial/(\partial x_{\text{plate}}) \int V_{\text{ext}}(\mathbf{r}; x_{\text{plate}})[|\psi_1(\mathbf{r})|^2 + |\psi_2(\mathbf{r})|^2]d\mathbf{r}$. The energy input rate is thus given by $\epsilon = -F\dot{x}_{\text{plate}}$. The value of ϵ (and also D) fluctuates in time due to the random nature of the turbulence. The sinusoidal motion of the plate-shaped potential also causes periodic fluctuation, as shown in Fig. 2(e). Therefore, we take the temporal average of these quantities, $\bar{\epsilon}$ and \bar{D} , over a sufficiently long time after the steady turbulent state is achieved. The inset in Fig. 3(a) shows $\bar{\epsilon}$ as a function of ν_{plate} for $g' = 1.02$ and 1.001 .

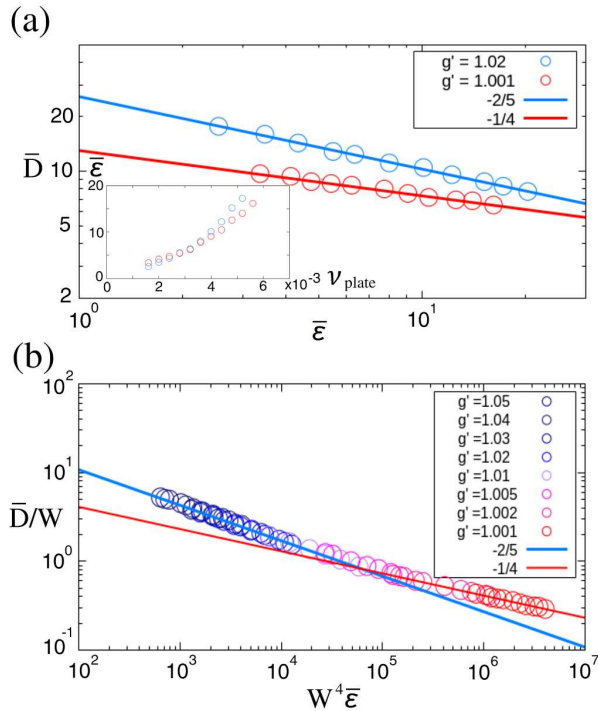


FIG. 3. (a) Typical domain size \bar{D} versus energy-input rate $\bar{\epsilon}$ for the steady turbulent state with $g' \equiv g_{12}/g = 1.02$ and 1.001 . The slopes of the lines are $-2/5$ and $-1/4$ for comparison with Eqs. (1) and (3). The inset shows $\bar{\epsilon}$ as a function of ν_{plate} . (b) \bar{D} and $\bar{\epsilon}$ are rescaled with respect to the interface width W for various values of g' . The plots collapse into a universal curve. The slopes of the lines are $-2/5$ and $-1/4$.

Now we are ready to investigate the KH scales in a turbulent superfluid in the classical and quantum regimes, as given in Eqs. (1) and (3). The result is shown in Fig. 3, which is the main result of this work. Figure 3(a) plots the typical domain size \bar{D} versus the energy-input rate $\bar{\epsilon}$ for $g' = 1.02$ and 1.001 . For $g' = 1.02$, the plots obey the power law $\propto \bar{\epsilon}^{-2/5}$, which agrees with the classical KH scale in Eq. (1). This implies that the two components are well separated, and the mechanism that sustains the domains against disintegration can be described by the interface tension in this region. For $g' = 1.001$, on the other hand, the plots in Fig. 3(a) follow the power law $\propto \bar{\epsilon}^{-1/4}$, which agrees with the KH scale in the quantum region in Eq. (3), implying that the mechanism to sustain domains is mainly the quantum kinetic pressure arising from the uncertainty principle. In this region, $\bar{D} \lesssim 10$ is smaller than $W \simeq (1.001 - 1)^{-1/2} \simeq 32$ and the interface tension of domains is not well-defined.

As discussed in deriving Eqs. (1) and (3), and numer-

ically confirmed in Fig. 3(a), the different power laws emerge, depending on the two length scales: the domain size \bar{D} and the interface width $W = (g' - 1)^{-1/2}$. Therefore, we use the rescaled domain size, \bar{D}/W . We can deduce that the crossover between the two power laws, Eqs. (1) and (3), always lies in the region of $\bar{D}/W \sim 1$. Note that Eq. (3) does not include W , and therefore, in the quantum KH region, $\bar{D} = c\bar{\epsilon}^{-1/4}$ can be rewritten as $\bar{D}/W = c(W^4\bar{\epsilon})^{-1/4}$ with a coefficient c that is independent of W . The \bar{D}/W versus $W^4\bar{\epsilon}$ line is thus universal in the region of the $-1/4$ power law, and the crossover to the region of the $-2/5$ power law always occurs at $\bar{D}/W \sim 1$; therefore it is expected that this line is universal over the entire region. Figure 3(b) plots \bar{D}/W versus $W^4\bar{\epsilon}$ for various values of g' . As expected, all the plots collapse into the universal curve, which bridges the two regions of the $-2/5$ and $-1/4$ power laws. Although \bar{D} and $\bar{\epsilon}$ are restricted to narrow ranges for each value of g' in the present numerical simulations, the rescaled plot in Fig. 3(b) significantly extends the effective ranges of \bar{D} and $\bar{\epsilon}$, which corroborates the existence of the two power laws in the superfluid KH scale.

Finally, we discuss the possible experimental realization of the present result. A box potential will be suitable to avoid complexity arising from the inhomogeneous $|\psi_1|^2 + |\psi_2|^2$ distribution in a harmonic potential. The stirring potential can be produced by a far-off-resonant laser beam. Shaking of an optical box can also be used to generate the turbulent state [25]. The typical size of the domains can be inferred from the imaging data, where the slice imaging of a three-dimensional distribution may be required [61]. It is difficult to measure the energy input rate directly; therefore, the support of numerical simulation is necessary, which provides the relation between the motion of the potential and the energy input rate, as in the inset in Fig. 3(a). The interaction g_{12} can be varied using the Feshbach resonance technique.

In conclusion, we have investigated the KH scale of domain sizes in immiscible two-component superfluids in a fully-developed turbulent state. We predict that two regions of the KH scale exist with different power laws, which reflect the quantum property of the system. Numerical simulations of the coupled GP equations were performed, and the typical domain size D was confirmed to obey the power laws with respect to the energy input rate ϵ . We found the universal function of the rescaled quantities D/W and $W^4\epsilon$, which connects the two regions of the quantum and classical KH scales. A possible extension of this study is a three-component system, in which the third component can change the interface tension of the other two components, resulting in emulsification.

This work was supported by JSPS KAKENHI Grant Number JP20K03804.

[1] A. N. Kolmogorov, Dokl. Akad. Nauk. SSSR **66**, 825 (1949).

[2] J. O. Hinze, AIChE J. **1**, 289 (1955).

- [3] See, e.g., U. Frisch, *Turbulence: The Legacy of A. N. Kolmogorov* (Cambridge University Press, Cambridge, UK, 1995).
- [4] P. H. Clay, Proc. Roy. Acad. Sci. (Amsterdam) **43**, 852 (1940).
- [5] R. Shinnar, J. Fluid Mech. **10**, 259 (1961).
- [6] C. A. Sleicher, AIChE J. **8**, 471 (1964).
- [7] K. Arai, M. Konno, Y. Matunaga, and S. Saito, J. Chem. Eng. Jpn. **10**, 325 (1977).
- [8] G. B. Deane and M. D. Stokes, Nature (London) **418**, 839 (2002).
- [9] P. Perlekar, L. Biferale, M. Sbragaglia, S. Srivastava, and F. Toschi, Phys. Fluids **24**, 065101 (2012).
- [10] R. Skartlien, E. Sollum, and H. Schumann, J. Chem. Phys. **139**, 174901 (2013).
- [11] P. Perlekar, R. Benzi, H. J. H. Clercx, D. R. Nelson, and F. Toschi, Phys. Rev. Lett. **112**, 014502 (2014).
- [12] X. Fan, P. H. Diamond, L. Chacón, and H. Li, Phys. Rev. Fluids **1**, 054403 (2016).
- [13] P. Perlekar, N. Pal, and R. Pandit, Sci. Rep. **7**, 44589 (2017).
- [14] M. E. Rosti, Z. Ge, S. S. Jain, M. S. Dodd, and L. Brandt, J. Fluid Mech. **876**, 962 (2019).
- [15] C. Nore, M. Abid, and M. E. Brachet, Phys. Rev. Lett. **78**, 3896 (1997); Phys. Fluids **9**, 2644 (1997).
- [16] S. R. Stalp, L. Skrbek, and R. J. Donnelly, Phys. Rev. Lett. **82**, 4831 (1999).
- [17] T. Araki, M. Tsubota, and S. K. Nemirovskii, Phys. Rev. Lett. **89**, 145301 (2002).
- [18] M. Kobayashi and M. Tsubota, Phys. Rev. Lett. **94**, 065302 (2005).
- [19] N. G. Parker and C. S. Adams, Phys. Rev. Lett. **95**, 145301 (2005).
- [20] A. W. Baggaley, J. Laurie, and C. F. Barenghi, Phys. Rev. Lett. **109**, 205304 (2012).
- [21] E. A. L. Henn, J. A. Seman, G. Roati, K. M. F. Magalhães, and V. S. Bagnato, Phys. Rev. Lett. **103**, 045301 (2009).
- [22] T. W. Neely, A. S. Bradley, E. C. Samson, S. J. Rooney, E. M. Wright, K. J. H. Law, R. Carretero-González, P. G. Kevrekidis, M. J. Davis, and B. P. Anderson, Phys. Rev. Lett. **111**, 235301 (2013).
- [23] W. J. Kwon, G. Moon, J.-Y. Choi, S. W. Seo, Y.-I. Shin, Phys. Rev. A **90**, 063627 (2014).
- [24] K. J. Thompson, G. G. Bagnato, G. D. Telles, M. A. Caracanhas, F. E. A. dos Santos, and V. S. Bagnato, Laser Phys. Lett. **11**, 015501 (2014).
- [25] N. Navon, A. L. Gaunt, R. P. Smith, and Z. Hadzibabic, Nature (London) **539**, 72 (2016).
- [26] S. P. Johnstone, A. J. Groszek, P. T. Starkey, C. J. Billington, T. P. Simula, and K. Helmerson, Science **364**, 1267 (2019).
- [27] N. Navon, C. Eigen, J. Zhang, R. Lopes, A. L. Gaunt, K. Fujimoto, M. Tsubota, R. P. Smith, and Z. Hadzibabic, Science **366**, 382 (2019).
- [28] S. Nazarenko and M. Onorato, J. Low Temp. Phys. **146**, 31 (2007).
- [29] T.-L. Horng, C.-H. Hsueh, S.-W. Su, Y.-M. Kao, and S.-C. Gou, Phys. Rev. A **80**, 023618 (2009).
- [30] R. Numasato, M. Tsubota, and V. S. L'vov, Phys. Rev. A **81**, 063630 (2010).
- [31] A. S. Bradley and B. P. Anderson, Phys. Rev. X **2**, 041001 (2012).
- [32] M. T. Reeves, T. P. Billam, B. P. Anderson, and A. S. Bradley, Phys. Rev. Lett. **110**, 104501 (2013).
- [33] T. Bland, G. W. Stagg, L. Galantucci, A. W. Baggaley, and N. G. Parker, Phys. Rev. Lett. **121**, 174501 (2018).
- [34] G. W. Stagg, N. G. Parker, and C. F. Barenghi, Phys. Rev. Lett. **118**, 135301 (2017).
- [35] N. G. Berloff and C. Yin, J. Low Temp. Phys. **145**, 187 (2006).
- [36] H. Takeuchi, S. Ishino, and M. Tsubota, Phys. Rev. Lett. **105**, 205301 (2010).
- [37] K. Fujimoto and M. Tsubota, Phys. Rev. A **85**, 033642 (2012); Phys. Rev. A **85**, 053641 (2012); Phys. Rev. A **88**, 063628 (2013); Phys. Rev. A **90**, 013629 (2014); Phys. Rev. A **93**, 033620 (2016).
- [38] M. Tsubota, Y. Aoki, and K. Fujimoto, Phys. Rev. A **88**, 061601(R) (2013).
- [39] B. Villaseñor, R. Zamora-Zamora, D. Bernal, and V. Romero-Rochín, Phys. Rev. A **89**, 033611 (2014).
- [40] D. Kobayakov, A. Bezett, E. Lundh, M. Marklund, and V. Bychkov, Phys. Rev. A **89**, 013631 (2014).
- [41] S. Kang, S. W. Seo, J. H. Kim, and Y. Shin, Phys. Rev. A **95**, 053638 (2017).
- [42] M. Karl, B. Nowak, and T. Gasenzer, Sci. Rep. **3**, 2394 (2013); Phys. Rev. A **88**, 063615 (2013).
- [43] K. Kudo and Y. Kawaguchi, Phys. Rev. A **88**, 013630 (2013); Phys. Rev. A **91**, 053609 (2015).
- [44] J. Hofmann, S. S. Natu, and S. Das Sarma, Phys. Rev. Lett. **113**, 095702 (2014).
- [45] S. De, D. L. Campbell, R. M. Price, A. Putra, B. M. Anderson, and I. B. Spielman, Phys. Rev. A **89**, 033631 (2014).
- [46] E. Nicklas, M. Karl, M. Höfer, A. Johnson, W. Muesel, H. Strobel, J. Tomkovič, T. Gasenzer, and M. K. Oberthaler, Phys. Rev. Lett. **115**, 245301 (2015).
- [47] L. A. Williamson and P. B. Blakie, Phys. Rev. Lett. **116**, 025301 (2016); Phys. Rev. A **94**, 023608 (2016); Phys. Rev. Lett. **119**, 255301 (2017).
- [48] A. Bourges and P. B. Blakie, Phys. Rev. A **95**, 023616 (2017).
- [49] M. Prüfer, P. Kunkel, H. Strobel, S. Lannig, D. Linneemann, C.-M. Schmied, J. Berges, T. Gasenzer, and M. K. Oberthaler, Nature (London) **563**, 217 (2018).
- [50] K. Fujimoto, R. Hamazaki, and M. Ueda, Phys. Rev. Lett. **120**, 073002 (2018).
- [51] H. Takeuchi, Phys. Rev. A **97**, 013617 (2018).
- [52] L. M. Symes, D. Baillie, and P. B. Blakie, Phys. Rev. A **98**, 063618 (2018).
- [53] See, e.g., L. D. Landau and E. M. Lifshitz, *Fluid Mechanics*, 2nd ed. (Butterworth-Heinemann, Oxford, 1987), Chap. VII.
- [54] P. Ao and S. T. Chui, Phys. Rev. A **58**, 4836 (1998).
- [55] R. A. Barankov, Phys. Rev. A **66**, 013612 (2002).
- [56] B. Van Schaeybroeck, Phys. Rev. A **78**, 023624 (2008); Phys. Rev. A **80**, 065601 (2009).
- [57] S. Choi, S. A. Morgan, and K. Burnett, Phys. Rev. A **57**, 4057 (1998).
- [58] See, e.g., C. J. Pethick and H. Smith, *Bose-Einstein condensation in dilute gases*, 2nd ed., Chap. 12. (Cambridge Univ. Press, Cambridge, 2008).
- [59] W. H. Press, S. A. Teukolsky, W. T. Vetterling, and B. P. Flannery, *Numerical Recipes*, 3rd ed. (Cambridge Univ. Press, Cambridge, 2007).
- [60] See Supplemental Material at <http://link.aps.org/supplemental/> for movies of the dynamics.

- [61] M. R. Andrews, C. G. Townsend, H.-J. Miesner, D. S. Durfee, D. M. Kurn, and W. Ketterle, *Science* **275**, 637 (1997).